Regulation of electron bunch arrival time for a continuous-wave linac: Exploring the application of the $\mathcal{H}_2$ mixed-sensitivity problem

Andrei Maalberg,* Michael Kuntzsch, and Klaus Zenker
Helmholtz-Zentrum Dresden-Rossendorf, 01328 Dresden, Germany

Eduard Petlenkov
Department of Computer Systems, Tallinn University of Technology, 19086 Tallinn, Estonia

(Received 31 January 2023; accepted 14 June 2023; published 10 July 2023)

Regulating the arrival time of electron bunches is a crucial step to improve the temporal resolution of accelerator-based pump-probe experiments. In this regard, an electron beam regulation method called beam-based feedback, has been shown to work well for stabilizing longitudinal beam properties on pulsed accelerator machines. Essentially, the method resembles a typical design of a proportional regulator, where the plant is represented by an electron beam response matrix, and where the inversion of such matrix produces the regulator. In recent years, however, linear accelerators that operate in a continuous-wave mode have received increasing attention. One of the key features of such machines is the improved statistics of measured data, which enables a high-resolution spectral analysis of the noise acting on the electron beam. This new insight allows us to reinterpret the electron beam regulation as a disturbance rejection goal, where the disturbance is based on measured frequency data. In this work, we show that the proportional beam-based feedback method has a principal performance limitation that becomes apparent by analyzing continuous-wave data. To improve this situation, we propose a regulator design that incorporates a dynamical disturbance model formulated in the context of the so-called $\mathcal{H}_2$ mixed-sensitivity problem. The designed regulator demonstrated excellent agreement between the model and measurements carried out at the continuous-wave linear accelerator ELBE and showed a potential to improve the proportional regulator approach.

DOI: 10.1103/PhysRevAccelBeams.26.072801

I. INTRODUCTION

Pump-probe experiments allow capturing the dynamics that occur in materials on an ultrafast timescale [1]. This is achieved by first exciting the dynamics in matter with an electromagnetic field of a pump pulse and then probing the excited matter with ultrashort photon pulses in a stroboscopic manner. To achieve a temporal resolution of less than a few tens of femtoseconds root-mean-square (rms) [2,3], these experiments rely on a tight synchronization between a pump source, which is typically an optical laser, and a source that generates the probes, e.g., a terahertz light source driven by an electron accelerator. Besides potential instabilities in the optical laser, the temporal stability of the electron accelerator, specifically of the underlying electron beam, is, therefore, of critical importance, which stresses the need to apply proper beam regulation.

Nowadays, an electron beam regulation method, called beam-based feedback, has been shown to work well for stabilizing longitudinal beam properties on pulsed accelerator machines [4–8]. Basically, the method first derives a matrix that denotes an electron beam response to variations in a radio-frequency (rf) field resonating inside an upstream accelerating structure, called cavity. The inverse of such matrix is then incorporated into the so-called low-level rf (LLRF) controller to allow adjusting the rf field based on the beam feedback. Finally, during an rf pulse, i.e., when the rf field is active, the LLRF controller can use the beam-based feedback to compensate for the noise acting on the beam. Putting aside the rf pulse details, the method resembles a typical design of a proportional regulator, where the beam response matrix represents a plant and where the plant inversion produces a regulator.

Contrary to the pulsed operation, a continuous-wave (cw) mode fills the accelerating cavities with a continuously driven rf field. That is, an rf field with a 100% duty cycle. For the user, such mode allows flexible electron bunch repetition rates and a high average beam current.

*a.maalberg@hzdr.de

This enables experiments that would otherwise be impossible to perform. In addition, a continuous train of electron bunches maintained for a sufficient amount of time greatly improves the statistics of experiment data. Consequently, linear accelerators (linacs) operating in the cw mode have received increasing attention in recent years. In particular, the construction of the Shanghai hard x-ray free electron laser facility (SHINE) began in 2018 [9]. The Linac Coherent Light Source II (LCLS-II) is nearing completion [10]. Moreover, the European X-ray Free Electron Laser (EuXFEL) considers a cw upgrade in the foreseeable future [11]. In this context, the electron linear accelerator for beams with high brilliance and low emittance (ELBE) [12] has been operating in cw mode for nearly 20 years and, therefore, represents a unique environment to test new algorithms and beamline components [13,14]. Hence, the results that are obtained at ELBE may have a substantial impact on the growing cw community.

Besides the user benefits, the improved statistics also help enhance feedback-related beam diagnostics. For example, a 1-s sampling of the rf field by a 50-kHz electron beam, i.e., a beam with a 50-kHz bunch repetition rate, provides data for a spectrum with a frequency resolution of 1 Hz. Since the electron bunches sample the inherent rf noise as well, a high-resolution spectral analysis of such noise becomes feasible. Clearly, this opens a possibility to reinterpret the electron beam regulation as a disturbance rejection goal, where the disturbance is based on the frequency-domain data of a measured electron beam signal. In this work, we exploit this opened possibility to address the regulation of an electron bunch arrival time. Specifically, we propose a solution that incorporates a dynamical disturbance model formulated in the context of the so-called $\mathcal{H}_2$ mixed-sensitivity problem. Even though design methods based on the $\mathcal{H}_2$ norm have already been used in the field of accelerators, e.g., to regulate an optical synchronization system [15–17], it is of interest to study the application of such methods to regulate the electron bunch arrival time on a cw machine. In this context, our designed regulator demonstrates excellent agreement between the model and measurements carried out at the cw linac ELBE and shows a potential to improve the proportional regulator.

The remainder of this paper is organized as follows: Section II starts by introducing the physics behind the beam-based feedback method and then continues the discussion from a control engineering point of view. Special attention is devoted to the performance limitation of the commonly used proportional regulator. In order to resolve the limitation, Sec. III proposes an improvement that is implemented in terms of a certain control engineering concept, called $\mathcal{H}_2$ mixed-sensitivity problem. Section IV evaluates the proposed improvement on the cw linear accelerator ELBE. Finally, Sec. V concludes the paper.

II. BEAM-BASED FEEDBACK METHOD

The state of a single particle is usually expressed relative to a reference trajectory, where the trajectory is assumed to be the path of a reference particle with nominal parameters. This allows us to define a Cartesian frame moving with the reference particle and providing the corresponding x, y, and z coordinates. Moreover, this concept can be generalized to represent an ensemble of particles, e.g., an electron bunch, by treating the ensemble as its center of mass. It is therefore common to describe the state as a six-dimensional phase space vector [18]

$$\rho = [x \quad x' \quad y \quad y' \quad z \quad \delta]^T, \tag{1}$$

where x, y, and z are the distances from the reference trajectory, $x' = \partial_x/\partial_z$ and $y' = \partial_y/\partial_z$ are the horizontal and vertical derivatives, respectively, and where $\delta = \Delta E/E_0$ is a relative deviation from the reference energy. To first order, the x, y, and z components can be decoupled, and thus, we can neglect the rest of the phase space and concentrate only on the longitudinal part

$$\rho_L = [z \quad \delta]^T. \tag{2}$$

The main beamline section that is able to change the longitudinal state ρ_L is called bunch compressor [18–20]. It is a combination of an rf cavity and a magnetic structure called chicane, formed by a minimum of four dipole magnets. The rf cavity is operated off-crest in order to chirp the bunch, i.e., to imprint an energy modulation that correlates with the longitudinal position z within the bunch. Correspondingly, the transfer map of the rf cavity can be expressed as

$$z(s_1) = z(s_0), \tag{3}$$

$$\delta(s_1) = \delta(s_0) + \frac{eA}{E_0}\cos\left(\frac{\omega}{c}z(s_0) + \phi\right), \tag{4}$$

where e is an elementary charge, c is the speed of light, and where A, ϕ, and ω are the amplitude, phase, and angular frequency of the rf cavity field, respectively. Beamline locations s_0 and s_1 mark the start and end of the rf cavity section, respectively. Then, by means of energy dispersion, the magnets of the chicane force the electrons to travel different paths, depending on the electron energy. Using only first-order terms, the corresponding transfer map is denoted as

$$z(s_2) = z(s_1) + R_{56}\delta(s_1), \tag{5}$$

$$\delta(s_2) = \delta(s_1), \tag{6}$$

where R_{56} is a first-order design parameter of the magnetic chicane that translates the energy modulation into a

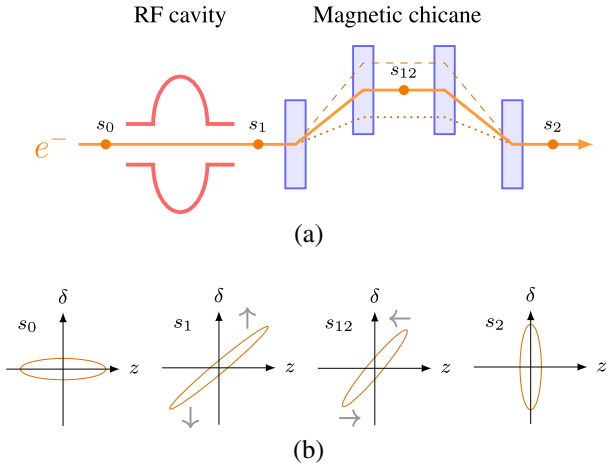

FIG. 1. Schematic of a bunch compressor exhibiting (a) the combination of an rf cavity and a magnetic chicane, as well as (b) the evolution of the longitudinal phase space of passing electron bunches.

longitudinal position change. Beamline locations s_1 and s_2 mark the start and end of the magnetic chicane section, respectively. Following this, the concept of the bunch compressor is illustrated in Fig. 1. It can be seen how electrons travel different paths through the magnetic chicane, depending on the energy received from the rf cavity. So in principle, the bunch compressor changes the longitudinal phase space of the electrons in a two-step sheering process: First, the rf cavity changes the energy distribution within the bunch; and second, the magnetic chicane alters the electron positions accordingly.

In case of arrival time, the electron bunch is represented by its center of mass. Thus, setting $z = 0$ and focusing only on the energy modulation introduced by the rf cavity allows transforming (3) into

$$\Delta\delta = \frac{eA}{E_0}\cos\phi. \tag{7}$$

This leads to a similar update of (5) featuring, in addition, a conversion to proper arrival time units

$$\Delta\tau = \frac{1}{v}R_{56}\Delta\delta, \tag{8}$$

where τ is the arrival time in seconds, and where $v \approx c$ and denotes the velocity of a relativistic electron bunch. So according to (7) and (8), where v and R_{56} are static for a given setting, the arrival time of the electron bunch can be regulated by modulating its energy. Usually, this modulation is performed with the help of an rf actuator, i.e., a control loop that allows setting and stabilizing the amplitude and phase of an rf field. To give a concrete example, the rf field control loop that is responsible for the bunch compressor at ELBE consists of a superconducting rf (SRF) cavity and a digital LLRF controller. The loop shows rms field stability of 0.005% in amplitude and 0.01° in phase [21]. Principally, this means that there are two rf field variables that the beam-based feedback can use to modulate the bunch energy. Yet according to (7), the rf field amplitude A is more linear than the phase ϕ. Moreover, changing ϕ changes the bunch compression, which is not desirable in this case. It is therefore reasonable to consider the phase ϕ a constant and define the output of the beam-based feedback regulator in terms of A exclusively, i.e.,

$$a = \frac{\Delta A}{A} \times 100, \tag{9}$$

where a is a change in percent with respect to the absolute rf field amplitude.

Meanwhile, the applied energy modulation leads to arrival time changes that can be measured downstream of the bunch compressor using an appropriate sensor. A bunch arrival time monitor (BAM) that is installed at ELBE may serve as an example of such sensor. It is able to measure the arrival time of the passing electron bunches with a time resolution of 4 fs rms at a bunch charge of 225 pC [22]. Finally, adding a beam-based feedback to regulate the electron bunch arrival time τ extends the bunch compressor schematic by cascaded control loops, i.e., the already existing rf field control loop becomes the so-called inner loop, whereas the added beam-based feedback forms the outer loop, see Fig. 2.

To design the corresponding beam-based feedback regulator, we may cast the extended bunch compressor to a single-input single-output (SISO) control problem, where τ is a controlled process variable and a is a control signal. The bunch compressor then represents a plant, where W_δ converts the control signal a to the absolute rf field amplitude A and G_δ and G_τ are (7) and (8), respectively. According to this simple design, the dynamics of the rf actuator are neglected. Instead, the beam-based

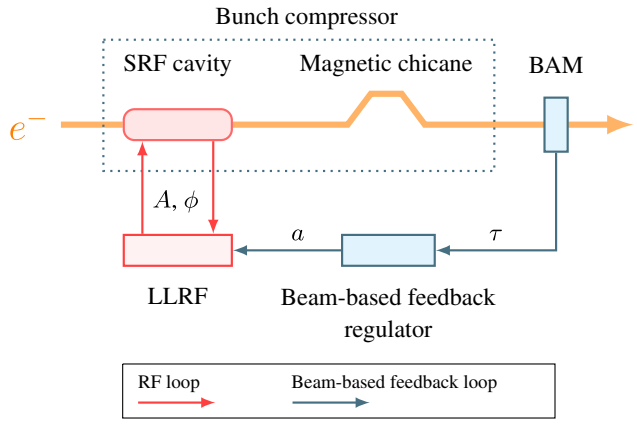

FIG. 2. Schematic of a bunch compressor extended by cascaded control loops to regulate an electron bunch arrival time.

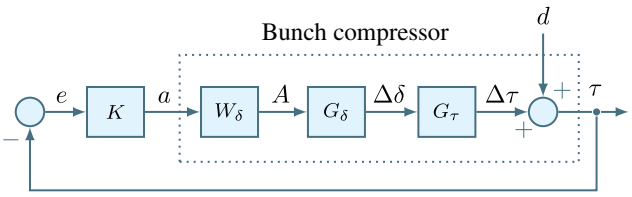

FIG. 3. Beam-based feedback regulation cast to a SISO control problem that is based on the first principles derived from the bunch compressor.

feedback regulator K acts directly on the bunch compressor in order to compensate for an error e, i.e., a negative impact of some unknown disturbance d on the process variable τ, see Fig. 3.

The origin of disturbance d is twofold: the rf noise inherent to the rf cavity [23] and the initial arrival time jitter of the passing electron bunches. In any case, the signal d represents a generalization, e.g., a unit step. To counteract such disturbance, it is straightforward to let K be an inverse of the bunch compressor plant, i.e.,

$$K = \gamma G_{BC}^{-1}, \tag{10}$$

where

$$G_{BC} = G_\tau G_\delta W_\delta = \frac{1}{v} R_{56} \frac{eA}{E_0} \cos\phi \frac{1}{100}, \tag{11}$$

and where γ is an additional gain to adjust the regulator performance. In fact, the value of G_{BC} can be determined analytically by evaluating (11) with corresponding parameters. Since we aim to regulate the ELBE accelerator, we evaluate G_{BC} with ELBE bunch compressor parameters from Table I. We are interested in finding the amount of variation in τ, given the input parameter $a = 1$. In this case, G_{BC} yields 776 fs/%. Essentially, the resulting scalar plant represents an electron beam response to variations in the rf field. The scalar variant can also be replaced by a matrix, provided there are more beam sensors available. The inverse of such matrix produces a proportional regulator K.

Even though the presented analytical formulation of G_{BC} captures the ultimate concept of the bunch compressor, it is still too simplified to match reality. The phase space of an electron bunch entering the bunch compressor may be far more complicated [24] than a simple ellipse illustrated in Fig. 1. This is why, a common engineering practice is to measure the beam response on a real machine, while

TABLE I. Bunch compressor parameters at ELBE.

Parameter	Value
rf field amplitude A of a chirping SRF cavity	7.27 MV
Off-crest rf field phase ϕ of a chirping SRF cavity	−21 deg
Reference energy E_0 of a magnetic chicane	28 MeV
R_{56} of a magnetic chicane	96 mm

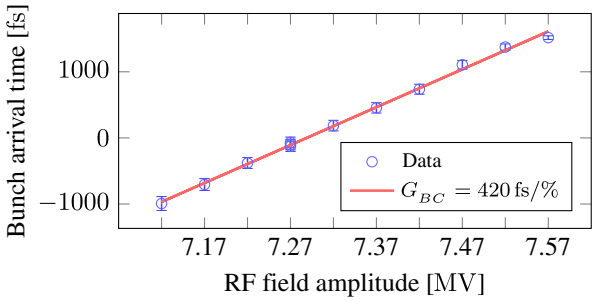

FIG. 4. Measuring the response of the electron bunch arrival time at ELBE, while changing the setpoint of the rf field amplitude $A = 7.27$ MV by steps of 50 kV.

changing the rf field in a stepwise manner. The ELBE bunch compressor, configured according to Table I, yields about 420 fs/% as a result of such measurement, see Fig. 4.

To cross-check the measured beam response, we use the final value theorem [25]. This theorem shows the final value of $e(t)$, i.e., the error of a closed-loop system, as t approaches infinity. So the idea of the cross-check is to first find γ that corresponds to the measured $e(\infty)$. Knowing the value of K that was applied during the measurement, we can then use the found γ to determine G_{BC} from (10). Therefore, given our assumption that disturbance d is a unit step, the theorem is defined as

$$e(\infty) = \frac{1}{1 + \lim_{s\to 0} L(s)}, \tag{12}$$

where s is the Laplace variable, and where the limit of a constant open-loop transfer function $L = G_{BC}K$ can be evaluated with the help of (10), yielding

$$\lim_{s\to 0} G_{BC}K = G_{BC}K = \gamma G_{BC} G_{BC}^{-1} = \gamma. \tag{13}$$

By substituting the limit in (12) with (13), we can express $e(\infty)$ as a function of γ, i.e.,

$$e(\infty) = \frac{1}{1+\gamma}. \tag{14}$$

Then, we define $e(\infty)$ as

$$e(\infty) \equiv \frac{\tau_o}{\tau_i}, \tag{15}$$

where τ_i and τ_o denote the integrated rms jitter of the electron bunch arrival time measured at ELBE with the proportional feedback off and on, respectively, see Fig. 5.

So by substituting $e(\infty)$ in (14) with (15), we are able to express γ as a function of the measured arrival time ratio, namely

$$\gamma = \frac{\tau_i}{\tau_o} - 1. \tag{16}$$

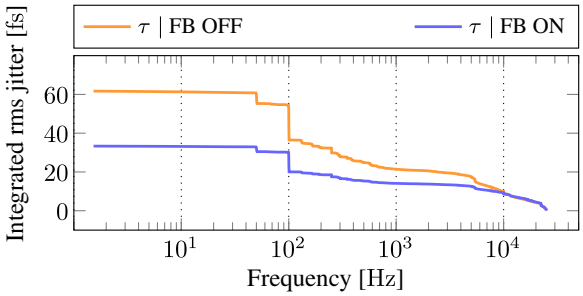

FIG. 5. Integrated rms jitter of the electron bunch arrival time measured at ELBE with the proportional feedback off and on.

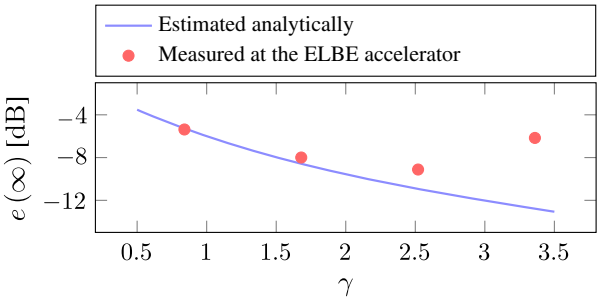

FIG. 6. Performance of a set of proportional regulators K, when G_{BC} is tied to the ELBE beam response of 420 fs/%, but γ is intentionally varied.

Finally, when evaluated with values from Table II, (16) and (10) yield $\gamma = 0.85$ and $G_{BC} = 427$ fs/%, respectively. The cross-checked value of G_{BC} indicates the validity of the beam response reported earlier.

Choosing $\gamma < 1$ to evaluate G_{BC} is characterized by a need to avoid triggering the degradation of the regulator performance. Specifically, increasing γ on the real machine does not reduce $e(\infty)$ according to an analytical estimation in (14) but rather causes (15) to substantially deviate, see Fig. 6.

The performance degradation observed on the real machine exposes the principal drawback of proportional regulators, namely the lack of bandwidth specification. Basically, such regulators apply control action across the whole frequency spectrum, which may cause interference with other control system components, mostly the actuators. For example, the above-mentioned rf actuator may exhibit dynamics with a certain bandwidth and gain margin. While the former property characterizes the speed of the actuator, the latter one defines how much gain can be additionally introduced into the closed-loop system before turning it unstable [25]. In this situation, the absence of a proper bandwidth specification makes the proportional regulator part of the actuator dynamics and, therefore, forces it to rely on the actuator gain margin. Derived from [21], the LLRF system at ELBE has a bandwidth of about 35 kHz and a gain margin of 11.6 dB. So theoretically, setting $\gamma \approx 3.8$ will consume the gain margin completely and, thus, turn the system unstable. Yet practically, we observe strong plant oscillations above 10 kHz already when $\gamma \approx 3.36$, see Fig. 7.

In this case, an *ad hoc* solution would be a trade-off between the noise suppression and plant stability. For example, setting $\gamma \approx 2.52$ achieves a suppression of the rms jitter by a factor of 3, i.e., only 22 fs rms jitter remains, while causing a moderate plant oscillation, see Fig. 8.

The displayed trade-off gives rise to the problem of finding a regulation approach that is able to achieve good noise suppression without compromising the plant's stability. In comparison to the displayed settings of the proportional regulator, the new approach should perform similarly to $\gamma \approx 0.85$ in the high-frequency range, but preferably better than $\gamma \approx 2.52$ in the low-frequency range. Therefore, in this study, we aim to take the actual noise explicitly into account. This means shifting the focus of attention from the analytical formulation to the size of a

TABLE II. Regulation of the electron bunch arrival time at ELBE using the proportional regulator.

Parameter	Value	Remark
τ_i	61.9 fs	rms integration range 1.5 Hz–25 kHz
τ_o	33.4 fs	rms integration range 1.5 Hz–25 kHz
K	0.002 fs/%	

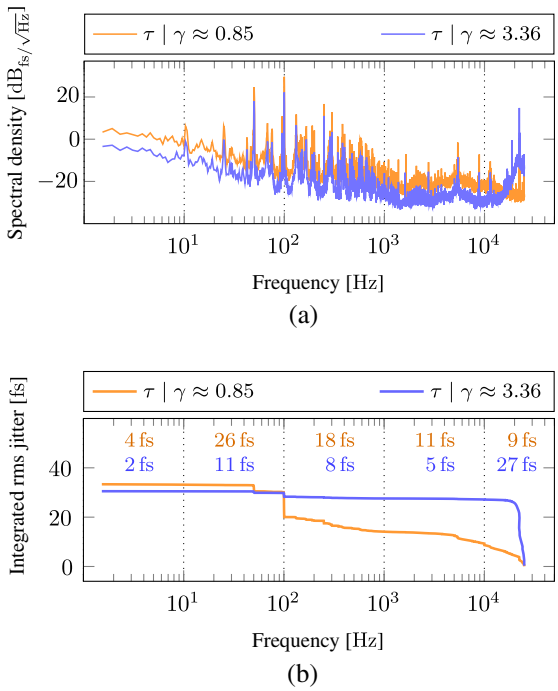

FIG. 7. Regulation of a 50-kHz electron beam at ELBE using a proportional regulator. (a) Setting $\gamma \approx 3.36$ triggers a pronounced plant oscillation above 10 kHz. (b) When calculating the rms jitter, this oscillation results in a large integration step, which negates the applied suppression effort, compared to a less aggressive regulator.

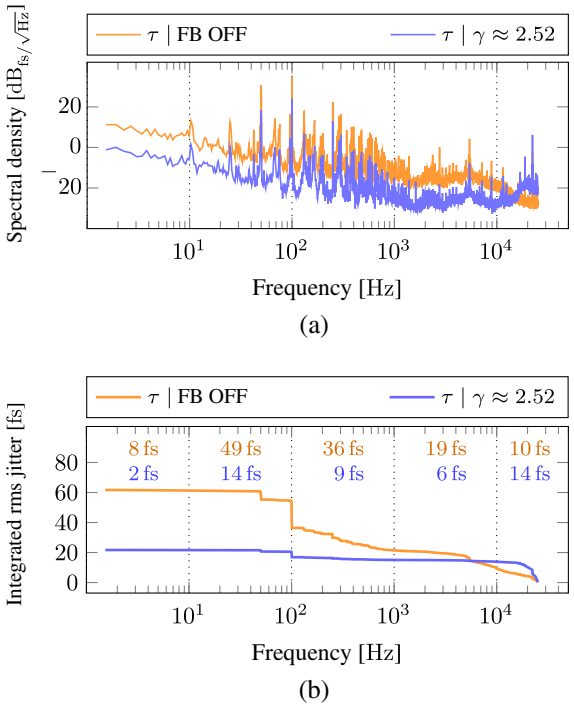

FIG. 8. Regulation of a 50-kHz electron beam at ELBE using a proportional regulator. (a) Setting $\gamma \approx 2.52$ causes a moderate oscillation above 10 kHz. (b) Nevertheless, the set γ allows suppressing the integrated rms jitter by a factor of 3.

concrete disturbance signal. So contrary to the proportional regulator, the new regulator K will try to compensate for the impact of a known disturbance d on the process variable τ. Obviously, the updated beam-based feedback method will have to ensure (i) a proper bandwidth definition in order to decouple the new regulator dynamics from the LLRF loop; (ii) a natural ability to incorporate a dynamical disturbance model inside the regulator design; (iii) a correspondence between the regulator performance criterion and the ultimate goal to suppress the rms value of the electron beam fluctuations.

To satisfy these requirements, we employ a regulator design method that is based on the $\mathcal{H}_2$ mixed-sensitivity problem [26,27]. On the one hand, this new regulator design represents a frequency-dependent optimization procedure. Hence, we can use a frequency-domain specification of the disturbance signal d. On the other hand, the designed regulator is expected not only to stabilize the plant model but also to minimize the rms fluctuations of the model output. Since the $\mathcal{H}_2$ norm of a model is directly related to the rms value of its output, minimizing such norm matches well our physical problem.

III. $\mathcal{H}_2$ MIXED-SENSITIVITY PROBLEM

The $\mathcal{H}_2$ norm of a transfer function G_d measures the rms response of the output when the input is driven by a white noise excitation [26,28]. The norm is denoted as

$$\|G_d\|_2 \triangleq \sqrt{\frac{1}{2\pi}\int_{-\infty}^{\infty} |G_d(j\omega)|^2 d\omega}, \tag{17}$$

where $|G_d(j\omega)|$ designates the magnitude frequency response of G_d evaluated at angular frequency ω. Suppose now that G_d defines the dynamics of a stochastic disturbance d that acts on the electron bunch arrival time τ. By using this transfer function together with its $\mathcal{H}_2$ norm as design specifications, the beam-based feedback regulator K can be aimed at reducing the sensitivity of τ to rms perturbations coming from d. Such interpretation allows formulating the beam-based feedback regulation in terms of the $\mathcal{H}_2$ mixed-sensitivity problem, see Fig. 9. According to such formulation, models G_d and G_n define the transfer functions of the electron beam disturbance d and the sensor measurement noise n, respectively. In addition, frequency weights W_S and W_{KS} help shaping the regulator performance and produce error signals w_S and w_{KS} that are used by an optimization procedure. Finally, as shown below, we define a specific bandwidth to decouple the designed regulator from the LLRF dynamics. This allows us to omit the rf field control loop from the design and continue using G_{BC} as the plant model.

Compared to the initial beam-based feedback control system, the main feature of the new design is the inclusion of the disturbance model G_d. This dynamical model is based on electron bunch arrival time data measured downstream of the ELBE bunch compressor. The model approximates the slopes of a linear spectral density derived from the data. That is, the model can be interpreted as a filter that shapes a theoretical white noise signal into the frequency content of the arrival time data. Importantly, to reflect the size of the measured signal, the $\mathcal{H}_2$ norm of the model is adjusted to satisfy

$$\|G_d\|_2 \approx \sqrt{\int_{f_1}^{f_2} [\tilde{\tau}(f)]^2 df}, \tag{18}$$

where $\tilde{\tau}(f)$ denotes the linear spectral density of the arrival time data τ in femtoseconds evaluated at frequency f, and

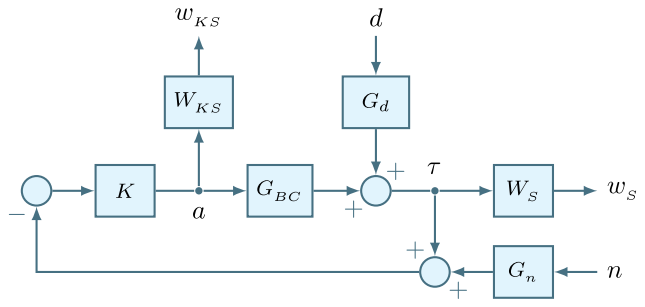

FIG. 9. Regulation of an electron bunch arrival time expressed in terms of the $\mathcal{H}_2$ mixed-sensitivity problem.

where $f_1 = 1$ Hz and $f_2 = 3.5$ kHz for a 50-kHz electron beam. Choosing 3.5 kHz as the upper integration limit has a couple of reasons. First, we know that the majority of the noise resides below 1 kHz [23], so we can use this information as a design constraint. Second, the designed $\mathcal{H}_2$ regulator aims to achieve decoupling from the LLRF dynamics [29], and this is accomplished by targeting a regulation bandwidth of 3.5 kHz, i.e., 1 order of magnitude lower than the 35 kHz bandwidth of the LLRF. Therefore, by choosing the locations of poles and zeros to reflect the frequency-domain shape of measured electron bunch arrival time noise, the transfer function G_d can be defined as

$$G_d(s) = \alpha \frac{s + z_0}{(s + p_0)(s + p_1)}, \tag{19}$$

where z_0 denotes the location of a zero at 500 rad/s, and where p_0 and p_1 are two pole locations at 50 and 5000 rad/s, respectively. The scalar parameter $\alpha = 4.1727 \times 10^3$ is used to satisfy (18). Hence, the norm $\|G_d\|_2$ yields 59 fs rms, which is, indeed, the majority of the noise when compared to the overall jitter of 62 fs rms. Accordingly, $G_d(s)$ represents an appropriately scaled second-order dynamical system with a 20-dB roll-off after 1 kHz, see Fig. 10.

By putting the disturbance model G_d into the context of the $\mathcal{H}_2$ mixed-sensitivity problem, the electron bunch arrival time signal can be expressed as

$$\tau = \underbrace{(1 + L)^{-1}}_{S} G_d d, \tag{20}$$

where $L = G_{BC}K$ and denotes an open-loop transfer function and S is a closed-loop transfer function called the sensitivity function. Inspection of (20) shows that we can reduce the sensitivity to disturbance input d by properly shaping S. Specifically, the shaping is performed in the frequency domain with the help of a frequency weight

$$W_S(s) = \frac{s/M_S + \omega_S}{s + \omega_S A_S}, \tag{21}$$

where $W_S(s)$ is a first-order low-pass filter, and where A_S and M_S define the low- and high-frequency gains, respectively. Parameter ω_S specifies an approximate bandwidth of the designed regulator. A typical guideline [26,27] is to make S small in the low-frequency range to achieve better disturbance rejection. For this purpose, we can use the low-frequency gain A_S to specify the desired suppression of G_d, see Fig. 11.

Another relevant closed-loop transfer function is related to the control signal a. This signal is generated by the beam-based feedback regulator K as a response to a perturbed electron bunch arrival time τ. Since the generated signal is used to manipulate the amplitude setpoint of the rf cavity field, our goal is to limit the control energy in order to avoid sensitivity to any unmodeled rf dynamics. This is accomplished by shaping the so-called input sensitivity function KS, which represents a link between the disturbance input d and control signal a, namely

$$a = KSG_d d. \tag{22}$$

Similar to the shaping of S, we shape the input sensitivity function KS using a frequency weight

$$W_{KS}(s) = \frac{s + \omega_{KS} A_{KS}}{s/M_{KS} + \omega_{KS}}, \tag{23}$$

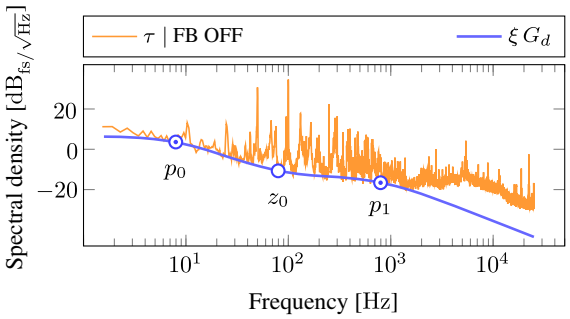

FIG. 10. Designing the disturbance model G_d to match the electron bunch arrival time noise up to 1 kHz. It is important to note that adherence to (18) makes the magnitude of G_d slightly greater than the noise shape. Consequently, for demonstration purposes, we use an extra parameter $\xi = 0.25$ to align the slopes.

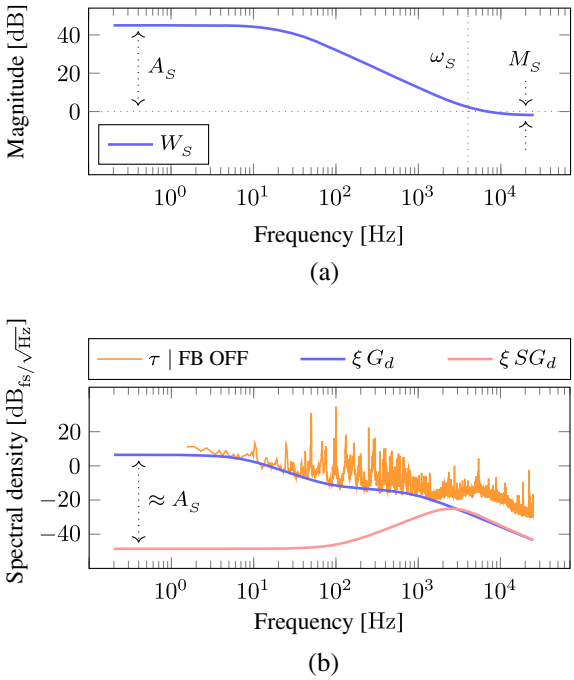

FIG. 11. Shaping the sensitivity function S using (a) a frequency weight W_S to (b) suppress the disturbance model G_d into its shaped closed-loop counterpart SG_d. For demonstration purposes, the extra parameter $\xi = 0.25$ aligns the slopes.

where $W_{KS}(s)$ is a first-order high-pass filter, and where A_{KS} and M_{KS} define the low- and high-frequency gains, respectively. Again, the parameter ω_{KS} is linked to the regulator bandwidth. The main objective is to increase the high-frequency roll-off of the closed-loop transfer function KSG_d by increasing the high-frequency gain M_{KS}. The steeper the roll-off, the less action is applied by the regulator beyond its bandwidth. Meanwhile, the low-frequency range of KSG_d follows the shape of the disturbance model G_d with a magnitude offset defined by G_{BC}^{-1}, see Fig. 12.

The sensor measurement noise model G_n is used to regularize the so-called sensor singularity at $\omega = \infty$. The fact is that the optimization procedure assumes that the sensor measurement τ has noise at every frequency, $\omega = \infty$ included. Yet the actual disturbance model G_d is defined by a strictly proper transfer function, such that

$$\omega \to \infty\colon\ G_d(j\omega) \to 0. \tag{24}$$

Consequently, to eliminate the singularity, the sensor measurement τ is redefined as $\tau + G_n n$, where G_n is a small nonzero constant. Interestingly, G_n can also be used as an effective bandwidth tuning knob. Together with ω_S and ω_{KS}, this parameter establishes the following regulator tuning procedure (i) Set parameters A_S, M_S, A_{KS}, and M_{KS} according to the specification, e.g., $A_S = 10^{\beta/20}$, where $\beta = -45$ dB; (ii) set parameters ω_S and ω_{KS} about equal to the bandwidth requirement or somewhat larger.

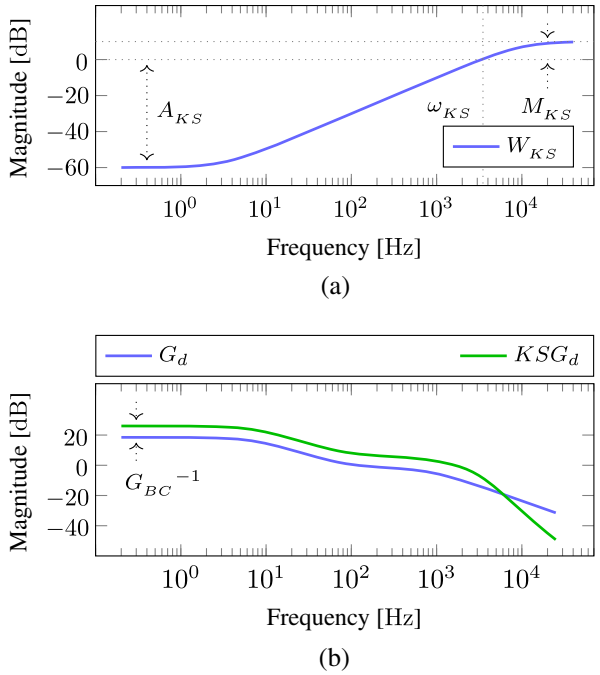

FIG. 12. Shaping the input sensitivity function KS using (a) a frequency weight W_{KS} to (b) increase the high-frequency roll-off of the closed-loop transfer function KSG_d.

Simultaneously, keep $\omega_S \le \omega_{KS}$; (iii) adjust the scalar G_n to align the bandwidth of the complementary sensitivity function $T = SL$ with the bandwidth requirement; (iv) adjust parameters ω_S and ω_{KS} as well as G_n to improve correspondence to the specification. Following this, Table III summarizes design parameters for a regulator that targets a bandwidth of about 4 kHz while suppressing the low-frequency noise by roughly 50 dB. By increasing the regulator bandwidth from 3.5 kHz to about 4 kHz, we aim to stress the decoupling test on the real machine.

Meanwhile, the synthesis of the $\mathcal{H}_2$ regulator is performed by a MATLAB function `h2syn` from the Robust Control Toolbox [30]. As the main input, the function expects a state-space model that resembles an interconnection of the blocks and signals displayed in Fig. 9, but with no regulator K to close the loop. As such, the interconnected model features inputs $[d\ n\ a]^T$ and outputs $[w_S\ w_{KS}\ \tau]^T$. This kind of interconnection is usually called a generalized, or augmented, plant. One possible way to prepare the generalized plant is to create the required block interconnection in SIMULINK, populate these blocks with model data, and then use a MATLAB function `linmod` [31] to extract a model of the generalized plant. Since the extracted model is in a state-space form, it is represented by matrices A, B, C, and D, which denote the system, input, output, and feedforward matrices, respectively. For the purpose of synthesizing the regulator K for this generalized plant, the function `h2syn` attempts to solve an optimization task. It amounts to finding a stabilizing regulator K that is able to minimize the $\mathcal{H}_2$ norm of a transfer function from the disturbance signal d to the error signals w, i.e.,

$$\begin{bmatrix} w_S \\ w_{KS} \end{bmatrix} = \begin{bmatrix} W_S S G_d \\ W_{KS} K S G_d \end{bmatrix} d. \tag{25}$$

Along with a state-space model of the synthesized regulator K, the function `h2syn` produces a full-state feedback gain K_u and an observer gain L_x, both returned as matrices. The relevance of these gains becomes evident, once we start discussing the relation between the states of the generalized plant and a real machine. In addition, the

TABLE III. $\mathcal{H}_2$ regulator design parameters.

Parameter	Value	Remark
$\|G_d\|_2$	59 fs	rms amount of expected noise
G_{BC}	420 fs/%	
G_n	0.00018	
A_S	0.0056	−45 dB
M_S	1.26	2 dB
ω_S	26 000 rad/s	4.14 kHz
A_{KS}	0.001	−60 dB
M_{KS}	3.16	10 dB
ω_{KS}	28 000 rad/s	4.46 kHz

manual regularization, which we apply with the help of the scalar G_n, allows us to switch off the automatic one applied by the function `h2syn`. Finally, the result of the regulator synthesis can be visualized in terms of the most relevant transfer functions, see Fig. 13.

As can be seen, the combination of S and KS sensitivity functions, often referred to as S/KS, plays the main role in shaping the desired behavior of the presented $\mathcal{H}_2$ mixed-sensitivity problem. Of course, this shaping adds a certain overhead to the design, because now the plant model is not merely the scalar G_{BC}, but the generalized plant, which includes the second-order disturbance model G_d, as well as the first-order shaping filters W_S and W_{KS}. As a result, we have a plant with four states, which essentially have no physical relation to the real machine and thus cannot be directly measured. To resolve this issue, the regulator K relies on state observation. That is, the regulator consists of two parts, namely (i) a dynamical state observer system, which estimates the state vector $\hat{x}$ and (ii) the above-mentioned full-state feedback matrix K_u, which uses the estimated states to produce an optimal control signal a, see Fig. 14. The matrices A, B, and C are derived from the state-space representation of the generalized plant obtained by the function `linmod`.

Mathematically, the observer-based structure of the beam-based feedback regulator K is expressed in a state-space form as

$$\dot{\hat{x}} = A\hat{x} + Ba + L_x(\tau - C\hat{x}), \tag{26}$$

$$a = K_u\hat{x}. \tag{27}$$

Converted to their discrete-time form, (26) and (27) can be implemented on a real-time field-programmable gate array-based digital platform [32]. By using the resulting digital implementation to close the loop on the real machine, we can finally validate the concept of the proposed beam-based feedback method. In particular, the ability to decouple the beam-based feedback from the LLRF dynamics in order to achieve greater noise suppression without triggering the unwanted plant oscillations. In addition, we can verify our performance estimations shown in Table IV.

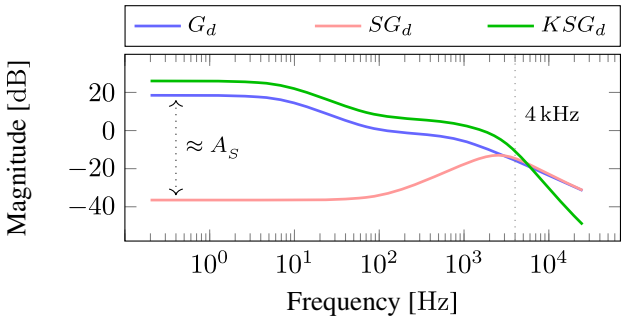

FIG. 13. $\mathcal{H}_2$ regulator visualized in terms of its transfer functions. The closed-loop transfer functions SG_d and KSG_d are clearly tailored to the disturbance model G_d.

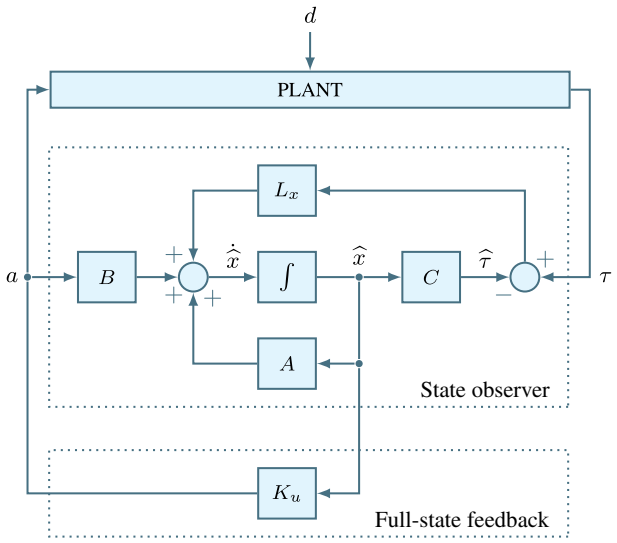

FIG. 14. Observer-based structure of the regulator K designed in terms of the $\mathcal{H}_2$ mixed-sensitivity problem.

IV. EVALUATING $\mathcal{H}_2$ REGULATOR AT ELBE

To evaluate the performance of the proposed $\mathcal{H}_2$ regulator, we conducted measurements on the cw linac ELBE. The layout of the measurement setup was equivalent to the proportional scheme displayed in Fig. 2. Accordingly, the bunch compressor was configured as shown in Table I. The compressed electron bunches with a bunch charge of 225 pC were then measured by the BAM with a time resolution of 4 fs rms. The result of this measurement demonstrated that in principle, the $\mathcal{H}_2$ regulator is able to achieve good noise suppression without triggering the plant oscillations, see Fig. 15. Specifically, the residual jitter amounts to 19 fs rms with the majority of it coming from frequency ranges, where the regulator is not active, i.e., above 1 kHz.

Moreover, the demonstrated correspondence between the model and arrival time data, both in open- and closed-loop cases, also applies to the control effort data. That is, the frequency-domain data of the control signal a follows the magnitude frequency response of the KSG_d transfer function up to 1 kHz. After this frequency, however, a flattens, as τ ascends to the peak located at approximately 5 kHz.

TABLE IV. Estimated performance parameters of the $\mathcal{H}_2$ beam-based feedback regulator.

Parameter	Value	Remark
$\|SG_d\|_2$	23 fs	rms amount of residual noise
$\|KSG_d\|_2$	0.14%	rms amount of regulation effort

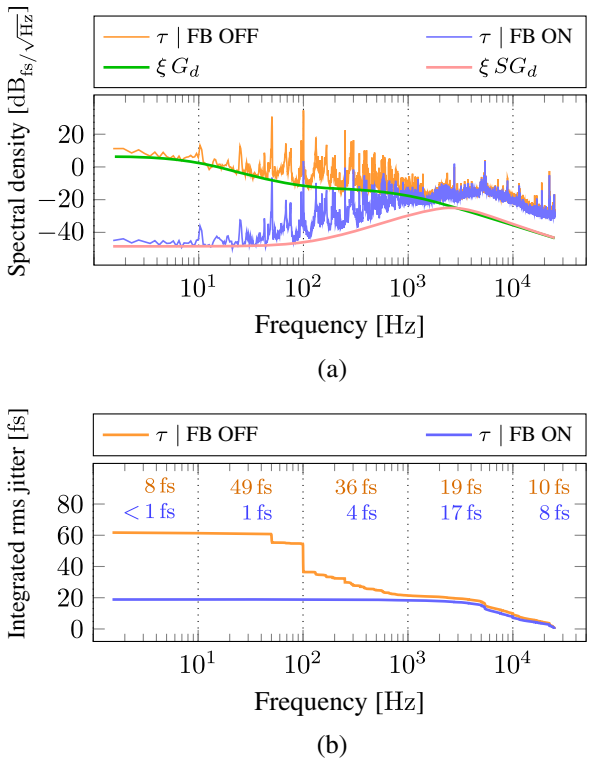

FIG. 15. Regulation of a 50-kHz electron beam at ELBE using the $\mathcal{H}_2$ regulator. (a) In the frequency domain, machine data exhibit correspondence with the model. (b) Simultaneously, integrated rms jitter data show that the regulator achieves good noise suppression below 1 kHz.

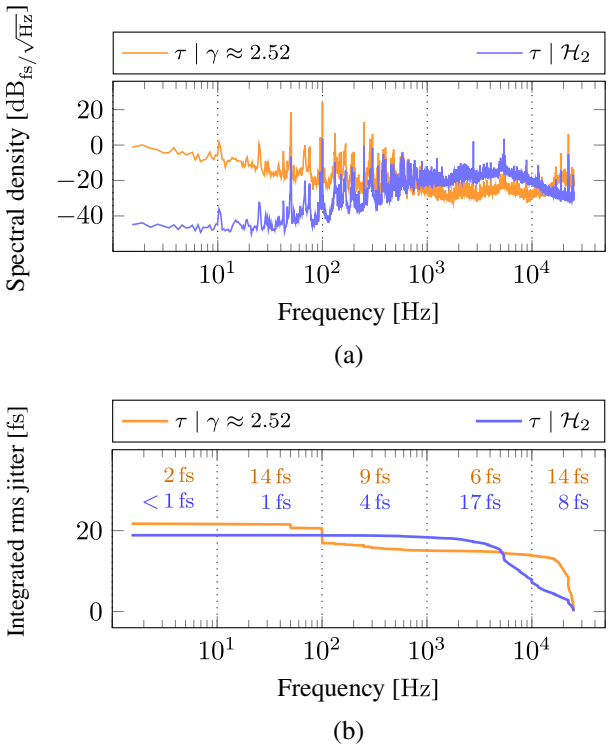

FIG. 17. Comparing performance between the proportional beam-based feedback method with $\gamma \approx 2.52$ and the $\mathcal{H}_2$ regulator. (a) The frequency domain clearly shows the different behaviors of both regulators depending on the frequency range. (b) This difference can also be seen while examining the band-limited amounts of the integrated rms jitter.

Once τ starts its descent, a can finally demonstrate the designed high-frequency roll-off, see Fig. 16. Also, the estimated parameters from Table IV turn out to be more conservative than our measurements. That is, the integration of a yields 0.13% rms, whereas the estimated parameter is 0.14% rms.

Therefore, the absence of the plant oscillations indicates a successful validation of the $\mathcal{H}_2$ regulator with respect to its decoupling from the LLRF dynamics. Compared to the proportional beam-based feedback method, the $\mathcal{H}_2$ regulator not only leaves the high frequencies intact but also shows superior suppression within its band of frequencies, see Fig. 17.

Finally, to better appreciate the achieved regulation of the electron bunch arrival time, one can view the

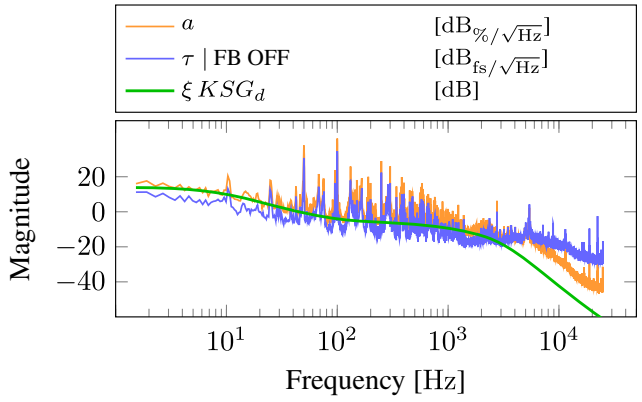

FIG. 16. Control effort to regulate a 50-kHz electron beam at ELBE using the $\mathcal{H}_2$ regulator. For demonstration, the extra parameter $\xi = 0.25$ aligns KSG_d with the slope of a.

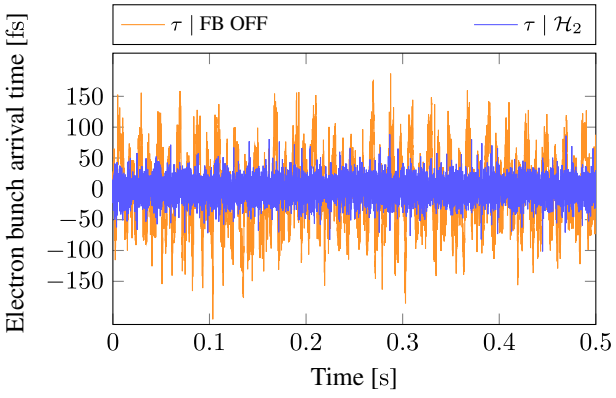

FIG. 18. Regulation of a 50-kHz electron beam at ELBE as observed in the time domain. The beam fluctuations are reduced using the $\mathcal{H}_2$ regulator.

result in the time domain, see Fig. 18. Indeed, large slow fluctuations disappear as the $\mathcal{H}_2$ regulator counteracts them, whereas small fast ones prevail. This is a natural outcome of applying a band-limited regulator that focuses on low-frequency range.

V. CONCLUSIONS

The increasing interest in superconducting linacs that operate in a cw mode enables the exploration of new capabilities in the design of a beam-based feedback method. The improved statistics of measured data allow reinterpreting the beam-based feedback as a disturbance rejection goal, where the disturbance is based on high-resolution frequency spectra of the measured data. Following this, S/KS disturbance rejection designs, such as the $\mathcal{H}_2$ mixed-sensitivity problem, become feasible.

In this work, we proposed a new design of a beam-based feedback regulator that exploits possibilities opened by the cw mode. The design seeks to minimize the noise of an electron bunch arrival time. Compared to a frequently used proportional regulator, the proposed design takes beam disturbance explicitly into account. Due to the low-frequency nature of this disturbance, it is possible to specify the design bandwidth accordingly and, thus, decouple the new regulator from the actuator dynamics. As a result, a specific plant instability, which is easily triggered by the proportional approach, poses no problem for the $\mathcal{H}_2$ regulator.

Despite its limited bandwidth, the designed $\mathcal{H}_2$ regulator demonstrated good noise suppression during an evaluation at the cw linac ELBE. Specifically, the electron bunch arrival time noise was reduced by a factor of 3, i.e., from 62 fs rms down to 19 fs rms. The corresponding frequency-domain data showed that a single regulation stage, which was installed at the end of the beamline, was sufficient to suppress low-frequency bands, i.e., from 1 Hz to 1 kHz, to less than 5 fs rms. The majority of the residual noise came then from the frequency bands, where the regulator was not active. Therefore, we expect to improve the overall suppression by carefully increasing the regulation bandwidth. In comparison, the above-mentioned plant instability prevented the proportional regulator from reducing the noise below 22 fs rms. Presumably, the use of multiple regulation stages, each working with $\gamma \approx 0.85$, could help overcome this situation. So in spite of its simplicity, improving the proportional regulation would require complex control system solutions, including more diagnostics, additional regulator hardware, and increased maintenance effort.

Another positive aspect of the proposed $\mathcal{H}_2$ design lies in its ability to estimate the size and frequency shape of important signals with the help of closed-loop transfer functions. In particular, functions S and KS can be tailored to a specific disturbance model in order to estimate residual noise and applied control effort, respectively. By displaying such frequency spectra together with their $\mathcal{H}_2$ norms, we showed an agreement between the model and measured data.

Therefore, having understood actual plant dynamics, we are now able to derive the right regulator parameters by (i) shaping a disturbance filter according to a measured noise spectrum and (ii) respecting a bandwidth limit given by a LLRF system. We expect this design procedure to be applicable to other cw machines as well. In addition, our implementation [32] could be transferred to these machines and tailored to their requirements.

Still, limiting the bandwidth of the new beam-based feedback method has an apparent downside. Namely, high-frequency noise cannot be addressed by the new regulator. Of course, suppressing such noise with an actuator that is based on a superconducting radio-frequency cavity with its inherently narrow bandwidth is problematic *per se*. Therefore, to counteract this negative scenario, a different design approach is required. For example, employing a normal conducting cavity that features a significantly wider bandwidth in order to specifically target the high-frequency noise [33,34]. Both regulators could then work in parallel, each targeting its own frequency range.

ACKNOWLEDGMENTS

The authors would like to thank Sven Pfeiffer from the German Electron Synchrotron (DESY) for fruitful discussions concerning beam-based feedback regulation. Special thanks goes also to Cagil Gümüs, Burak Dursun, and Łukasz Butkowski for their help with the MTCA.4 firmware framework. This work was partially funded by the Estonian Research Council Grant No. PRG658.

[1] B. Green *et al.*, High-field high-repetition-rate sources for the coherent THz control of matter, Sci. Rep. **6**, 22256 (2016).

[2] H. Schlarb, Techniques for pump-probe synchronisation of FSEC radiation pulses, in *Proceedings of the 21st Particle Accelerator Conference, Knoxville, TN, 2005* (IEEE, Piscataway, NJ, 2005), pp. 59–63.

[3] S. Kovalev, B. Green, T. Golz, S. Maehrlein, N. Stojanovic, A. S. Fisher, T. Kampfrath, and M. Gensch, Probing ultrafast processes with high dynamic range at 4th-generation light sources: Arrival time and intensity binning at unprecedented repetition rates, Struct. Dyn. **4**, 024301 (2017).

[4] W. Koprek, C. Behrens, M. K. Bock, M. Felber, P. Gessler, K. Hacker, H. Schlarb, C. Schmidt, B. Steffen, S. Wesch, S. Schulz, and J. Szewinski, Intra-train Longitudinal Feedback for Beam Stabilization at FLASH, in *Proceedings of 32nd International Free Electron Laser Conference Malmö, Sweden* (JACoW, Geneva, Switzerland, 2010), pp. 537–543.

[5] C. Schmidt, M. Bock, W. Koprek, S. Pfeiffer, H. Schlarb, and W. Jałmużna, Feedback strategies for bunch arrival time stabilization at FLASH towards 10 fs, in *Proceedings of 33rd International Free Electron Laser Conference,*

Shanghai, China (SINAP, Shanghai, China, 2011), pp. 531–534.

[6] S. Pfeiffer, C. Schmidt, M. K. Bock, H. Schlarb, W. Jalmuzna, G. Lichtenberg, and H. Werner, Fast feedback strategies for longitudinal beam stabilization, in *Proceedings of the 3rd International Particle Accelerator Conference, New Orleans, LA, 2012* (IEEE, Piscataway, NJ, 2012).

[7] S. Schulz, I. Grguraš, C. Behrens, H. Bromberger, J. T. Costello, M. K. Czwalinna, M. Felber, M. C. Hoffmann, M. Ilchen, H. Y. Liu, T. Mazza, M. Meier, S. Pfeiffer, P. Predki, S. Schefer, C. Schmidt, U. Wegner, H. Schlarb, and A. L. Cavalieri, Femtosecond all-optical synchronization of an X-ray free-electron laser, Nat. Commun. **6**, 5938 (2015).

[8] A. Rezaeizadeh, T. Schilcher, and R. S. Smith, Adaptive robust control of longitudinal and transverse electron beam profiles, Phys. Rev. Accel. Beams **19**, 052802 (2016).

[9] Z. Zhao, D. Wang, Z. Yang, and L. Yin, SCLF: An 8-GeV CW SCRF linac-based x-ray FEL Facility in Shanghai, in *Proceedings of 38th International Free Electron Laser Conference, Santa Fe, NM* (JACoW, Geneva, Switzerland, 2018), pp. 182–184.

[10] F. Zhou, C. Adolphsen, A. Benwell, G. Brown, D. H. Dowell, M. Dunning, S. Gilevich, K. Grouev, G. Huang, B. Jacobson, X. H. Liu, A. Miahnahri, F. Sannibale, J. Schmerge, and T. Vecchione, Commissioning of the SLAC Linac Coherent Light Source II electron source, Phys. Rev. Accel. Beams **24**, 073401 (2021).

[11] R. Brinkmann, E. Schneidmiller, J. Sekutowicz, and M. Yurkov, Prospects for CW and LP operation of the European XFEL in hard X-ray regime, Nucl. Instrum. Methods Phys. Res., Sect. A **768**, 20 (2014).

[12] P. Michel, The radiation source ELBE at the Forschungszentrum Dresden-Rossendorf, in *2008 IEEE Nuclear Science Symposium Conference Record, Dresden, Germany* (IEEE, New York, 2008), pp. 3078–3080.

[13] A. Bellandi, Ł. Butkowski, B. Dursun, A. Eichler, Ç. Gümüş, M. Kuntzsch, A. Nawaz, S. Pfeiffer, H. Schlarb, C. Schmidt, K. Zenker, and J. Branlard, Online detuning computation and quench detection for superconducting resonators, IEEE Trans. Nucl. Sci. **68**, 385 (2021).

[14] H. Vennekate, A. Arnold, P. Lu, P. Murcek, J. Teichert, and R. Xiang, Emittance compensation schemes for a superconducting rf injector, Phys. Rev. Accel. Beams **21**, 093403 (2018).

[15] M. Heuer, G. Lichtenberg, S. Pfeiffer, H. Schlarb, C. Schmidt, and H. Werner, Modeling of the master laser oscillator phase noise for the European XFEL using fractional order systems, in *IFAC Proc.* Vol. 47 (2014), p. 9235.

[16] M. Schütte, A. Eichler, H. Schlarb, G. Lichtenberg, and H. Werner, Decentralized output feedback control using sparsity invariance with application to synchronization at European XFEL, in *Proceedings of 60th IEEE Conference on Decision Control, Austin, TX* (IEEE, New York, 2021), pp. 5723–5728.

[17] M. Schütte, A. Eichler, H. Schlarb, G. Lichtenberg, and H. Werner, Convex synthesis of robust distributed controllers for the optical synchronization system at European XFEL, in *Proceedings of IEEE Conference on Control Technology and Applications, Trieste, Italy* (IEEE, New York, 2022), pp. 1061–1067.

[18] A. Wolski, *Beam Dynamics in High Energy Particle Accelerators* (Imperial College Press, London, England, 2014).

[19] P. Emma, *Bunch compression, Handbook of Accelerator Physics and Engineering*, 2nd ed. (World Scientific Publishing Co. Pte. Ltd., Hackensack, NJ, 2013), pp. 334–337.

[20] P. Emma, X-band RF harmonic compensation for linear bunch compression in the LCLS, Stanford Linear Accelerator Center, Stanford University, Stanford, CA, Technical note, Report No. LCLS-TN-01-1, 2001.

[21] K. Zenker, Ç. Gümüş, M. Hierholzer, P. Michel, S. Pfeiffer, H. Schlarb, C. Schmidt, R. Schurig, R. Steinbrück, and M. Kuntzsch, MicroTCA.4-based low-level RF for continuous wave mode operation at the ELBE Accelerator, IEEE Trans. Nucl. Sci. **68**, 2326 (2021).

[22] M. Kuntzsch, K. Zenker, A. Maalberg, A. Schwarz, M. Czwalinna, and J. Kral, Update of the bunch arrival time monitor at ELBE, in *Proceedings of 13th International Particle Accelerator Conference, Bangkok, Thailand* (JACoW, Geneva, Switzerland, 2022), pp. 260–262.

[23] A. Maalberg, M. Kuntzsch, and E. Petlenkov, Simulation of RF noise propagation to relativistic electron beam properties in a linear accelerator, IFAC Pap. **53**, 348 (2020).

[24] U. Lehnert, P. Michel, R. Schurig, A. Aksoy, P. Evtushenko, and J. Krämer, Bunch compression of the low-energy ELBE electron beam for super-radiant THz sources, in *Proceedings of the 5th International Particle Accelerator Conference, IPAC2014, Dresden, Germany* (JACoW, Geneva, Switzerland, 2014), pp. 1123–1125.

[25] N. Nise, *Nise's Control Systems Engineering*, global ed. (John Wiley & Sons, Ltd, Chichester, West Sussex, England, 2015).

[26] S. Skogestad and I. Postlethwaite, *Multivariable Feedback Control: Analysis and Design*, 2nd ed. (John Wiley & Sons, Ltd, Chichester, West Sussex, England, 2005).

[27] H. Kwakernaak, $\mathcal{H}_2$-optimization—theory and applications to robust control design, *IFAC Proc.* Vol. 33 (2000), p. 437.

[28] S. Boyd and C. Barratt, *Linear Controller Design: Limits of Performance* (Prentice-Hall Inc., Hoboken, NJ, 1991).

[29] A. Maalberg, M. Kuntzsch, and E. Petlenkov, Regulation of the linear accelerator ELBE exploiting continuous wave mode of a superconducting RF cavity, in *Proceedings of the 2022 American Control Conference, Atlanta, GA* (IEEE, New York, 2022), pp. 5346–5353.

[30] G. Balas, A. Packard, M. Safonov, and R. Chiang, Next generation of tools for robust control, in *Proceedings of the 2004 American Control Conference, Boston, MA* (IEEE, New York, 2004), pp. 5612–5615.

[31] MathWorks, linmod: Extract continuous-time linear state-space model around operating point, Available online at https://se.mathworks.com/help/simulink/slref/linmod.html (2023) [accessed: March 31, 2023].

[32] A. Maalberg, M. Kuntzsch, and E. Petlenkov, Real-time regulation of beam-based feedback: Implementing an FPGA solution for a continuous wave linear accelerator, Sensors **22**, 6236 (2022).

[33] S. Pfeiffer, J. Branlard, Ł. Butkowski, M. Hierholzer, M. Hoffmann, K. Honkavaara, H. Schlarb, C. Schmidt, S. Schreiber, M. Vogt, J. Zemella, and M. Fakhari, Status update of the fast energy corrector cavity at FLASH, in *Proceedings of 29th Linear Accelerator Conference, LINAC2018, Beijing, China* (JACoW, Geneva, Switzerland, 2018), pp. 112–114.

[34] S. Pfeiffer, Ł. Butkowski, M. Czwalinna, B. Dursun, C. Gerth, B. Lautenschlager, H. Schlarb, and C. Schmidt, Longitudinal intra-train beam-based feedback at FLASH, in *Proceedings of 39th Free Electron Laser Conference, FEL2019, Hamburg, Germany* (JACoW, Geneva, Switzerland, 2019), pp. 346–349.